17th World Conference on Earthquake Engineering, 17WCEE
Sendai, Japan - September 13th to 18th 2020

REDUCED ORDER MODELING OF HYSTERETIC STRUCTURAL RESPONSE AND APPLICATIONS TO SEISMIC RISK ASSESSMENT

D. Patsialis [(1)], A.A. Taflanidis [(2)]

[((1)] *Graduate Student, Department of Civil and Environmental Engineering and Earth Sciences, University of Notre Dame, dpatsial@nd.edu*

[(2)] *Associate Professor, Department of Civil and Environmental Engineering and Earth Sciences, University of Notre Dame, a.taflanidis@nd.edu*

Abstract

Modern seismic risk assessment applications require simulation of structural behavior for different levels of earthquake shaking through time-history analysis. This behavior can be strongly inelastic/hysteretic and evaluating it through high-fidelity finite element models (FEMs) introduces a significant computational burden. A reduced order modeling approach is discussed here to alleviate this burden. The reduced order model is developed using data from the original high-fidelity FEM. Static condensation is first used to obtain the condensed stiffness matrix and linear equations of motion for the dynamic degrees of freedom (DoFs). The restoring forces, prescribed by the linear stiffness matrix, are then substituted with hysteretic ones, by replacing the linear springs connecting each of the DoFs with hysteretic springs. Different models are examined for the latter, ranging from peak-oriented to Masing to Bouc-Wen type of hysteresis. Springs connecting all DoF combinations are examined and their parameters are calibrated by comparing the reduced order model time-history to the time-history of the initial FEM for a range of different excitations. This is posed as a least squares optimization problem, which is solved through global optimization algorithms. The characteristics for each of the considered springs are separately selected, leading to a large dimensional design vector for this optimization, and an efficient solution is facilitated through a sequential, hierarchical approach. The excitations utilized for the reduced order model calibration are carefully selected, so that nonlinear characteristics of the FEM are appropriately excited to support the tuning of all the important hysteretic spring features. The accuracy and the computational savings of the calibrated reduced order model are examined for seismic risk assessment applications by comparing them to the FEM predictions. A stochastic ground motion model is used to describe the seismic hazard and the accuracy for different levels of intensity is separately examined. Finally, a multi-fidelity Monte Carlo method is used to establish a computationally efficient unbiased estimator of any output quantity of the FEM. This method leverages the low-cost, potentially biased, reduced order model evaluations to accelerate the risk assessment estimation within a Monte Carlo setting, and occasionally uses resources from the computationally expensive high-fidelity FEM to establish unbiased calculations. This multi-fidelity approach provides high accuracy risk estimates, as if only the FEM was used in the calculations, but simultaneously leverages both the computational efficiency of the reduced order model as well as its correlation to the FEM to offer a substantial improvement with respect to the computational effort. Both the latter features, computational efficiency and correlation to FEM predictions, are essential for this multi-fidelity approach to work well, and it is shown that the proposed reduced order model tuning accommodates both well.

Keywords: reduced order modeling; seismic risk assessment; sequential optimization; multi-fidelity approach

1. Introduction

Under strong seismic excitations, structural systems exhibit inelastic, hysteretic behavior and the evaluation of their dynamic response requires development of nonlinear finite element models (FEMs). For seismic risk assessment and loss estimation [1], this is typically performed using either concentrated plasticity models, using nonlinear hinges to represent the behavior in locations of anticipated damages, or distributed inelasticity models, using a fiber discretization of the cross sectional area of all structural elements and adopting appropriate nonlinear constitutive laws for the material behavior. The computational burden of using such models is significant, especially for applications, like probabilistic risk (and loss) assessment, that estimate risk by, usually, adopting a Monte Carlo (MC) approach that entails a significant number of nonlinear time history responses, for different excitations and different intensity levels of ground shaking. Reduced order modeling offers an alternative modeling approach to alleviate this computational burden. Formally, reduced order models (ROMs) simplify the physics-based description of the original FEM through some form of condensation of the initial degrees of freedom and equations of motion. For facilitating the desired computational efficiency for seismic risk assessment applications, this condensation needs to be coupled with an approximation of the nonlinear response characteristics. The calibration of the nonlinear properties of the resulting hysteretic ROM should be performed using data from the original nonlinear FEM, with ultimate objective that the reduced order approximate model matches closely the high-fidelity one for excitations similar to the ones that is intended to be used for. Then, the calibrated ROM replace the high fidelity FEM for estimating the seismic risk. Though noteworthy attempts do exist for calibrating ROMs by comparing to nonlinear FEMs [2, 3], they do have some limitations. Study [2] was constrained to shear-type of structural models and performed the ROM tuning using nonlinear static analysis. Study [3] addressed any planar structural model and performed tuning using nonlinear response history analysis (NLRHA), but was primarily constrained to simple dynamic excitations for the tuning, while it adopted a simplified parameterization of the nonlinear hysteretic force approximation and performed validation for limited excitations.

This study extends these efforts and presents a comprehensive approach for tuning and validation of hysteretic ROMs [4]. Linear characteristics of the ROM are obtained using static condensation of the initial FEM, while nonlinear characteristics are calibrated by comparing response to the nonlinear FEM response under different earthquake acceleration time-histories. A sequential formulation of the associated least squares optimization problem is established so that the approach can accommodate adoption of complex descriptions for the ROM hysteretic forces. Validation is performed with respect to seismic risk estimation for different seismicity scenarios extending to lower and higher intensity excitations. While the use of low-fidelity ROMs is offering a substantial MC speedup in this context, the corresponding estimation might be biased when compared against the one established using higher-fidelity, higher accuracy, numerical models. For that reason, a multi-fidelity Monte Carlo (MC) [5, 6] method is also utilized. This approach is leveraging, instead of entirely replacing, a small number of the computationally expensive response estimations offered by the FEM, to establish unbiasedness, while uses a significant number of the low-cost response approximations of the ROM, to speed-up the estimation. The number of simulations for each of the models is optimally selected [7], based on the correlation between them, to minimize the variance of the MC estimator, for a given computational budget. The benefits of using ROM in risk assessment applications and of utilizing the multi-fidelity MC are demonstrated in an illustrative example that considers two structures, corresponding to different heights and materials, with high-fidelity FEMs developed in OpenSees.

2. Reduced order model formulation

2.1 Condensed structural model

In this study, emphasis is placed on planar structural models (as also shown in Fig. 1) and under the common modeling assumptions of infinite axial floor rigidity and zero rotational mass for individual nodes, the model can be condensed to one degree of freedom (DoF) per story. The corresponding stiffness matrix is obtained

through static condensation of the original FEM. Let $\mathbf{x}_s \in \mathbb{R}^n$ denote the vector of displacements for each floor relative to the base. The equation of motion of the linear condensed model is:

$$\mathbf{M}_s\ddot{\mathbf{x}}_s + \mathbf{C}_s\dot{\mathbf{x}}_s + \mathbf{K}_s\mathbf{x}_s = -\mathbf{M}_s\mathbf{R}_s\ddot{x}_g \tag{1}$$

where $\mathbf{M}_s$ and $\mathbf{K}_s$ are the $n \times n$ mass and stiffness matrices, respectively, both chosen to match the FEM ones, $\mathbf{C}_s$ is the $n \times n$ damping matrix, modeled using the same assumptions as for the FEM, $\mathbf{R}_s \in \mathbb{R}^n$ is the vector of earthquake influence coefficients and $\ddot{x}_g \in \mathbb{R}$ represents the acceleration of the base. Eq. (1) facilitates a match of the linear response between the ROM and the high-fidelity FEM.

2.2 Representation Through linear springs

Consider now the combination of all n_t=n(n-1) springs connecting the degrees of freedom to each other and to the ground. The spring connecting degrees of freedom i and j is denoted by s_{ij} where i=1, …, n; j=0, i+1, …, n. Index j=0 is used to represent the connection to the ground. Let $\mathbf{T}_s$ be the $n_t \times n$ connectivity matrix relating the relative displacements at the ends of each spring δ_{ij} to vector $\mathbf{x}_s$. Each row of $\mathbf{T}_s$ corresponds to a separate spring s_{ij} and has all elements zero apart from the ith element equal to 1 and the jth element when $j \neq 0$ equal to -1. If $\boldsymbol{\delta}$ is the vector with relative spring displacements, δ_{ij}, then $\boldsymbol{\delta}$=$\mathbf{T}_s\mathbf{x}_s$. The condensed stiffness matrix can be equivalent expressed as:

$$\mathbf{K}_s = \mathbf{T}_s^T\mathbf{K}_l\mathbf{T}_s \tag{2}$$

where $\mathbf{K}_l$ is the diagonal matrix with elements:

$$k_{ij}^l = [\mathbf{K}_s]_{ij} \text{ if } j \neq 0 \quad \& \quad k_{i0}^l = [\mathbf{K}_s]_{ii} - \sum_{k\neq i,k=1}^{n}[\mathbf{K}_s]_{ik} \text{ if } j = 0 \tag{3}$$

where $[.]_{ij}$ represents the ijth element of a matrix. This spring formation with spring characteristics k_{ij}^l given by Eq. (3) matches exactly the linear FEM stiffness.

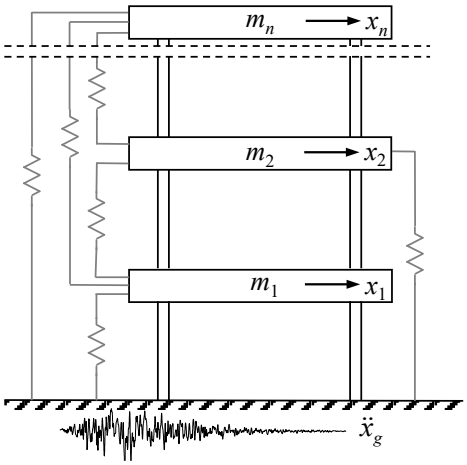

Fig. 1 – Structural model and representation through springs (in grey) connecting the different Dofs.

2.3 Hysteretic model

The formulation of the hysteretic ROM is established by modeling spring forces f_{ij} to be nonlinear instead of the linear ones $k_{ij}^l\delta_{ij}$. Each nonlinear spring force is defined as a function of the spring displacement δ_{ij} parameterized through n_t dimensional vector $\mathbf{q}_{ij}$. Typical choices for this function [2, 3] include piecewise linear elastic-perfectly plastic (PP) or peak-oriented (PO) models, generalized Masing models (GM) and Bouc-Wen (BW) models. The hysteretic spring forces for all aforementioned models are given by

$$f_{ij} = a_{ij}k_{ij}^l\delta_{ij} + (1-a_{ij})g_{ij}(\delta_{ij}) \tag{4}$$

where the hysteretic function $g_{ij}(.)$ depends on the exact hysteretic model used. Details for the formulation of the four hysteretic models can be found in [2].

Not all spring s_{ij}, though, need to be necessarily modeled as hysteretic (i.e., inelastic) ones. Some can be considered as linear. We will use notation $\{.\}$ to represent the combination of all springs (or their parameters) that are modeled to be hysteretic. Size of $\{s_{ij}\}$, i.e. number of inelastic springs, is denoted n_c. The connectivity matrix for $\{s_{ij}\}$ is denoted by $\mathbf{T}_c$ and is obtained by retaining only the rows of $\mathbf{T}_s$ that correspond to elements of $\{s_{ij}\}$. The equation of motion of the hysteretic ROM are

$$\mathbf{M}_s\ddot{\mathbf{x}}_s + \mathbf{C}_s\dot{\mathbf{x}}_s + \mathbf{T}_c^T diag(\{g_{ij}(\delta_{ij})\}) + \mathbf{K}_s^{rem}\mathbf{x}_s = -\mathbf{M}_s\mathbf{R}_s\ddot{x}_g \tag{5}$$

where $diag(\mathbf{a})$ stands for diagonal matrix with diagonal elements corresponding to vector $\mathbf{a}$ and $\mathbf{K}_s^{rem}$ is matrix corresponding to linear spring components, given by

$$\mathbf{K}_s^{rem} = \mathbf{K}_s - \mathbf{T}_c^T diag(\{(1-a_{ij})k_{ij}^l\})\mathbf{T}_c \tag{6}$$

Structural model represented by Eq. (5) matches exactly the linear FEM response. The match to the nonlinear FEM response depends on how $\ddot{x}_g^h$ well the chosen hysteretic function approximates the actual hysteretic behavior and on the selection of parameters $\{\mathbf{q}_{ij}\}$ of that function. That selection is discussed next.

3. Calibration of inelastic parameters

3.1 Formulation of calibration problem

Calibration of the model parameters pertains to selection of $n_l n_c$ dimensional vector $\mathbf{q}$ corresponding to $\{q_{ij}\}$. This is established by comparing nonlinear time-history responses between the hysteretic ROM and the nonlinear FEM. Comparison should consider different earthquake excitations; since objective of the ROM development is to replace the FEM for seismic loss estimation, its calibration should consider same operational conditions, that is earthquake excitations, instead of simplified excitations.

To formalize this calibration, let [; h=1,.., n_h] represent the set of eartquakes considered and $\mathbf{y}$=[y_l; l=1,…,n_y] the set of response outputs used in the calibration. The selection of the earthquake set should excite all essential components of the FEM nonlinear behavior, providing sufficient information for the calibraiton of the corresponding nonlinear ROM springs. This can be accomplished if a large number of excitations is examined. These do not need to be distinct, rather scaling of the same earthquakes can be also considered. For the set of response outputs, since seismic losses exhibit sifnigicant sensitivity to drift engineering demand parameters and, furthermore, inelastic structural behavior typically results in residual drifts, response output vector $\mathbf{y}$ should include at least inter-storey drifts, preferably for all floors. Also, for the hth earthquake, calibration is performed over time duration T_h, typically extending over the entire duration of the earthquake. The output from NLRHA for the FEM for each earthquake and time instance will be denoted by $y_{FEM}^l(t_r^h \mid \ddot{x}_g^h)$. For the ROM, corresponding notation will be $y_{ROM}^l(t_r^h \mid \ddot{x}_g^h, \mathbf{p})$. The objective function is given by the weighted mean squared discrepancy

$$F(\mathbf{q}) = \frac{1}{n_h}\sum_{h=1}^{n_h} w_h \left(\frac{1}{n_y}\sum_{l=1}^{n_y} w_h^l \left[\frac{1}{T_h}\int_0^{T_h} w^{hl}(t) e_{hl}^2(t \mid \mathbf{q}) dt \right] \right); \; e_{hl}(t \mid \mathbf{q}) = (y_{FEM}^l(t \mid \ddot{x}_g^h) - y_{ROM}^l(t \mid \ddot{x}_g^h, \mathbf{q})) \tag{7}$$

where w_h is the weight for each earthquake, w_l^h is the weight for each output for the hth earthquake, $w^{hl}(t)$ is the weight per time instance for the lth output and hth earthquake, and $e_{hl}(t|\mathbf{q})$ represents the discrepancy between the FEM and ROM time-histories. Selection of $\mathbf{q}$ is finally posed as the nonlinear constrained optimization problem

$$\mathbf{q}^* = \underset{\mathbf{q}\in[\mathbf{q}_{\min}, \mathbf{q}_{\max}]}{\arg\min} \; F(\mathbf{q}) \quad \text{such that } \min(\text{eig}(\mathbf{K}_s^{rem})) > 0 \tag{8}$$

where $[\mathbf{q}_{min}, \mathbf{q}_{max}]$ represents the box-bounded constraint for $\mathbf{q}$ and $\min(\text{eig}(\mathbf{K}_s^{rem}))$ corresponds to the minimum eigenvalue for matrix $\mathbf{K}_s^{rem}$. The constraint for that eigenvalue being positive guarantees that the ROM corresponds to a stable structural model.

3.2 Sequential optimization

The optimization problem of Eq. (8) is nonconvex and has a costly objective function involving n_h NLRHAs for the ROM. Solution of this optimization is performed here through a two-step approach, combining an efficient global optimization (EGO) as a first step [9] to search the entire $[\mathbf{q}_{min}, \mathbf{q}_{max}]$ domain and identify a candidate global optimum and a gradient-based optimization (NPSOL) as a second step [10] to further improve upon this solution. Genetic algorithms (GA) [11] can be alternatively considered for the global optimization step.

For problems, though, with large dimensional vector $\mathbf{q}$ the cost associated with the global search over domain $[\mathbf{q}_{min}, \mathbf{q}_{max}]$ can be prohibitively high. Since that global search is important due to the non-convex nature of the problem, a sequential optimization is proposed here. The basic idea is to gradually and hierarchically increase the number of spring features that are considered as inelastic, starting from the most important ones, and at each iteration optimize only for the newly added spring parameters. In the final optimization stage, a simultaneous gradient-based optimization of all nonlinear spring parameters is established, with initial point the values identified through the global optimization sub-problems in the previous iterations, in order to take into account, the correlation between the independently optimized springs. The optimization workflow is described in detail in [4].

3.3 Selection of type of hysteresis and of earthquake excitations

For selecting the type of hysteresis, all possible models should be considered, for example PO, PP, GM and BW discussed earlier, and the one corresponding to the smaller objective function value $F(\mathbf{q}^*)$ should be adopted. Model parsimony can be incorporated in the analysis, if desired, using Bayesian inference, for example the well-known Bayesian information criterion. The selection of the earthquake excitation set $[\ddot{x}_g^h\ ;\ h=1,..,\ n_h]$, now, is critical for the proper calibration of the spring inelastic parameters. This set should excite all essential components of the FEM nonlinear behavior, providing sufficient information for the calibraiton of the corresponding nonlinear reduced order model springs. These do not need to be distinct, rather scaling of the same earthquakes can be also considered. The range of excitation intensities should encompass the operating conditions that the reduced order model will be used for. More details about the selection of appropriate earthquake excitations can be found in [4].

4. Illustrative example

4.1 Details of structural models and simulation characteristics

For the illustrative example, two structures are used. For both structures, the nonlinear FEM is developed in OpenSees [12] using fiber modeling approach for the describing hysteretic behavior, with the selection of fiber elements following recommendations from [13]. The first structure, denoted as S_1 corresponds to a nine story benchmark structure, discussed in detail in [14]. Material characteristics are: modulus of elasticity $E=1.99\ 10^5$ MPa for both beams and columns, yield stress for the columns 345 MPa and 248 MPa for the beams, using the values proposed in [14]. For modeling material inelastic behavior, the Giuffre'-Menegotto-Pinto model with isotropic strain hardening is chosen for the steel fibers. For the latter model, the values suggested in [15] are used for the cyclic curvature parameter and for the parameters defining isotropic strain hardening in compression and tension, while the strain hardening ratio is taken as 0.02. Total number of fiber elements per section is set to 24. Damping matrix $\mathbf{C}_s$ is modeled through Rayleigh damping assumption with damping ratios selected as 2% for 1st and 3rd modes. The fundamental period for the S1 structure is 2.274 s. The second structure, denoted herein as S_2, is the three-story symmetric concrete MRF building described in detail in [2]. The only difference from [2] is that the reinforcement ratio for exterior columns is increased to 1.5% (compared to the 1% initially used) to better reflect modern code-compliant structures. As in [2] one of

the exterior three-bay frames is examined, with each bay having 6.5 m span and each story having 3.5 m height. The OpenSees FEM fiber model is constructed using 20 fibers for the confined core and 15 fibers for the unconfined section per each direction. For the constitutive material laws for concrete and steel, OpenSees materials Concrete02 [16] and Steel02 [17] are used respectively. It should be noted here that the concrete material that was used is a linear tension softening material, that also incorporates strength and stiffness degradation. Damping matrix Cs is modeled through Rayleigh damping assumption with damping ratios selected as 5% for 1st and 3rd modes. The fundamental period for structure S_2 is 0.57 s.

The ROMs are developed in the SIMULINK simulation environment using guidelines discussed in [2] for performing the NLRHA, adopting accelerator mode for shortening model simulation time. For a time-step of 0.01 s and using Newmark's average acceleration for numerical integration and for excitation of duration of 40 s (this corresponds to Loma Prieta excitation used later in calibration) the computational time required for the NLRHA in a desktop with 4core Xeon 3.1GB processor is 111 s and 39 s for the OpenSees model corresponding to structures S_1 and S_2 respectively. The corresponding simulation times under the same simulation characteristics (same numerical integrator and time-step) for the ROM are 0.20 s and 0.28 s for structures S_1 and S_2 respectively when using the BW hysteretic model, and 0.18 s and 0.15 s for structures S_1 and S_2 respectively when using the PP hysteretic model. These two represent the most and least, respectively, computationally intensive models from the ones considered. The comparison of computational effort demonstrates the significant computational savings that the ROM can offer; a 100 to 600-fold reduction for computational effort is established.

4.2 Reduced order model calibration

For the calibration, six different recorded ground motions are considered, taken from the PEER Strong Motion database [18]: Kobe, Northridge and Loma Prieta, earthquakes that correspond to high intensity excitations for both structures (shown in [4]), and ChiChi, Friuli and Imperial Valley, which are low intensity excitations (also shown in [4]). For these excitations, three different calibration scenarios are examined. The first one, denoted as SC_1, uses the first three high intensity excitations (n_h=3); the second, denoted as SC_2, considers additionally scaled versions of the three recorded excitations using scaling 1.25 (n_h=6); the third one, denoted as SC_3, considers all six excitations (n_h=6). All four different hysteretic models discussed in Section 2.3 are considered. No degrading characteristics are being incorporated for structure S_1 but degradation is incorporated in the models for structure S_2.

The reduced order models calibrated through each of the considered scenarios are denoted, respectively by D_1, D_2 and D_3. Only inter-storey drift ratios of every floor were used in the calibration stage. For each earthquake, the strong ground motion duration with discretization dt=0.01 is assumed for defining t_r. Considering further the different weights appearing in the objective function definition in this study, the definition for $w^{hl}(t)$ focuses on the strong ground motion duration, so that matching to EDP peaks, which typically occur during that duration, is prioritized. The cumulative energy of the earthquake excitation up to time instance t is considered for this purpose, given by:

$$\varepsilon_h(t) = \frac{\pi}{2g}\int_0^t \left(\ddot{x}_g^h(t)\right)^2 dt \tag{9}$$

For t=T_h this energy corresponds to the Arias intensity $I_a^h = \varepsilon_h(T_h)$ of the excitation. Weight $w^{hl}(t)$ is set equal to 1 for all time instances corresponding to cumulative energy between 5%-97.5% of the total energy of the excitation

$$w^{hl}(t) = \begin{cases} 1 & \text{if } 0.05 \le \varepsilon_h(t)/\varepsilon_h(T_h) \le 0.975 \\ 0 & \text{else} \end{cases} \tag{10}$$

This choice weights equally all time-instances during the strong ground motion duration, the latter taken to extend up to the 97.5% of the total excitation energy compared to the common definition of 95% of the total excitation energy. This extension is chosen here to capture better residual drift responses. Finally, weight w_h^l

introduces a normalization for the different response quantities and in this study is chosen as the variance of the FEM response $y^l_{FEM}(t^h_r \mid \ddot{x}^h_g)$

$$w^l_h = \frac{1}{T_h}\int_0^{T_h} w^{hl}(t)(y^l_{FEM}(t \mid \ddot{x}^h_g))^2 dt \tag{11}$$

Table 1: Optimal value of the objective function $F(\mathbf{q}^*)$ for the different hysteretic models and main calibration scenarios for each of the two structures

Hysteretic model	Structure S_1			Structure S_2		
	SC_1	SC_2	SC_3	SC_1	SC_2	SC_3
PO	0.1737	0.1949	0.1672	0.1371	0.1395	0.1974
PP	0.0531	0.0599	0.0473	0.2457	0.2371	0.2879
GM	0.0377	0.0460	0.0238	0.1725	0.2032	0.2115
BW	0.0202	0.0206	0.0197	0.1612	0.1934	0.1854
Linear ROM	2.0860	2.3905	1.2932	1.4331	1.5024	1.2972

Table 2: Value for $F(\mathbf{q})$ for the three different calibration scenarios for the three different calibration cases using the BW and PO models for structures S_1 and S_2 respectively.

Structure	ROM	Calibration scenario		
		SC_1	SC_2	SC_3
S_1 [*BW* hysteresis]	D_1	**0.0202**	0.0228	0.0236
	D_2	0.0205	**0.0206**	0.0255
	D_3	0.0224	0.0259	**0.0197**
S_2 [*PO* hysteresis]	D_1	**0.1371**	0.1982	0.2564
	D_2	0.1562	**0.1395**	0.2347
	D_3	0.1423	0.312	**0.1974**

Results for the calibration of the ROM are reported in Table 1 and Table 2. In Table 1, the resultant objective function values for the main calibration scenarios are reported, along with results for the linear ROM (all springs considered linear). It is evident, that BW and PO models outperform the other ones for S_1 and S_2 structure, respectively, and are the only one considered for the remainder of the discussions. In addition, it is clear that the values of the objective function for S_2 are worse compared to S_1. This should be attributed to a more complex nonlinear behavior of reinforced concrete structures, as explained in [4].Table 2 presents the objective function value $F(\mathbf{q})$, evaluated for the three different designs D_1, D_2 and D_3 for each

calibration scenario, for both structures and for the BW and PO hysteresis. Results show that performance is similar across all different calibrations, especially for SC_2 and SC_3, indicating that even the initial selection of the three earthquakes has sufficient information to identify all spring nonlinearities.

4.3 Validation of reduced order model for seismic risk assessment

Validation is first examined looking at time-history response. The first validation step briefly discusses time-history response for an excitation that was not part of the initial calibrations scenario. Figure 2 presents time-histories for the nonlinear OpenSees FEM, the linear FEM and the calibrated ROM for top floor inter-story drift and top floor acceleration (columns of the figure) for both structures (rows of the figure) for the Kocaeli earthquake ground motion. Very good agreement is reported across the entire time-history for the calibrated ROM (compare to the poor agreement for the linear model), extending to both peak and overall responses and to both EDPs. This offers a first validation of the robustness of the calibration procedure: for different excitations and even for EDPs that were not explicitly considered at the calibration stage, the resultant models offer the same quality of match to the nonlinear OpenSees FEM as the match observed for the excitations and EDPs these models have been optimized against.

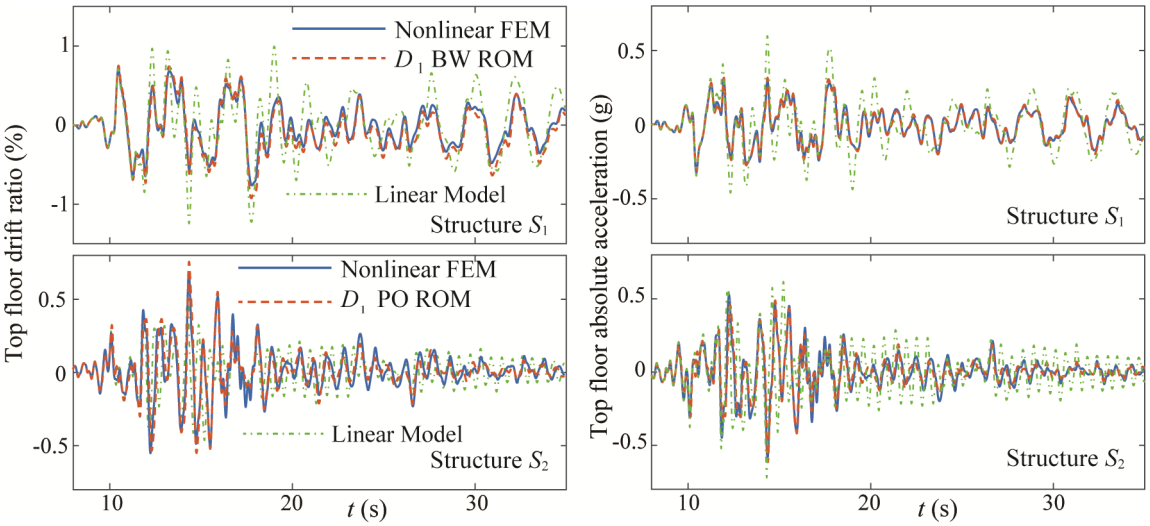

Fig. 2: Comparison of time-history responses for an inter-story drift and top floor acceleration for the both structures (rows of the figure) for Kocaeli earthquake ground motion. Results for nonlinear Opensees FEM, best ROM and linear ROM shown.

The more interesting comparison is, of course, with respect to loss estimation, instead of individual excitations. For describing the seismic hazard for this comparison the stochastic ground motion model developed recently by Vlachos et al. [19] is used. Four different seismicity scenarios are considered corresponding to combinations of moment magnitude M=[6.5, 7.5] and rupture distance R=[20, 50] km. With respect to local site conditions (required by ground motion model) the shear wave velocity at top 30 m of soil 600 m/s. Seismic risk is expressed with respect to the complementary cumulative distribution function (CCDF), corresponding to the probability that engineering demand parameter EDP_j will exceed specific threshold β, $P[EDP>\beta]$, for a range of thresholds corresponding to probabilities [0.01-1], for each seismicity scenario. For each seismicity scenario, 1000 samples were used to calculate the CCDF curves. Figures 3 and 4 present results for structures S_1 and S_2 respectively for selective EDP_s (first floor drift and top floor acceleration). Results in the figures show that the proposed calibration approach facilitates very good agreement with respect to risk estimates across different thresholds for all seismicity scenarios and EDPs. Exception is the top floor acceleration for structure S_2, for low values of the threshold acceleration, for which larger discrepancies are evident. These large discrepancies can be particularly observed for the lowest seismicity scenario examined (M=6.5, R=50km). Such larger discrepancies can be avoided by putting some preference in matching acceleration response for lower intensity excitations at the calibration stage. The

effects of this choice should be carefully examined, though, since it will inevitably reduce the approximation quality for large intensity excitations. Another way to increase accuracy and actually establish an unbiased estimator for accelerations and inter-story drifts is a multi-fidelity Monte Carlo estimation, described in the following section.

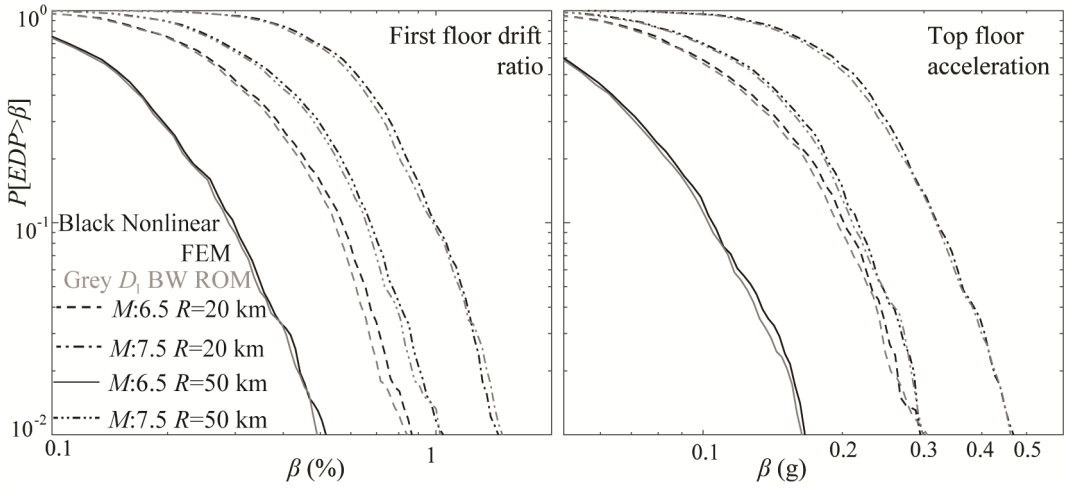

Fig. 3: Comparison of CCDF curves from the high-fidelity OpenSees and best ROM corresponding to calibration D_1 for structure S_1. Results for selective seismicity scenarios and EDP_s are shown.

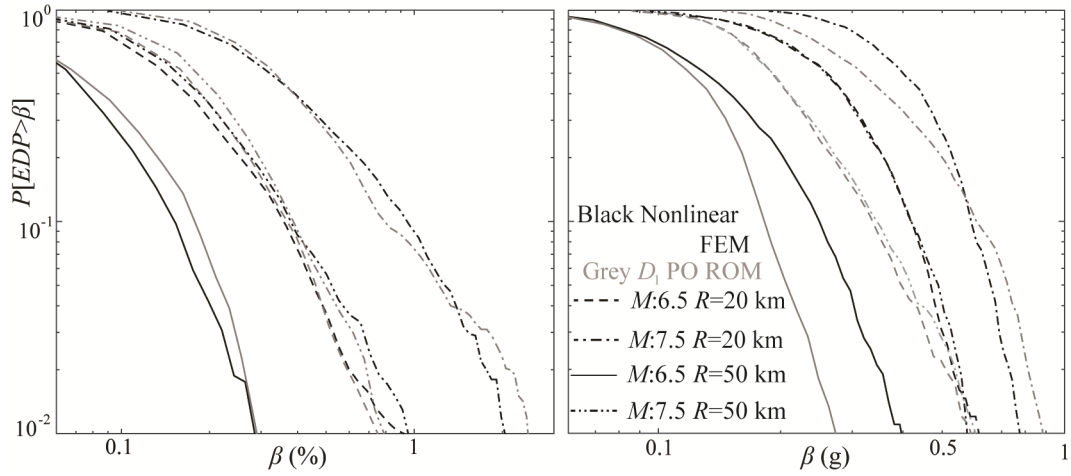

Fig. 4: Comparison of CCDF curves from the high-fidelity OpenSees and best ROM corresponding to calibration D_1 for structure S_2. Results for selective seismicity scenarios and EDP_s are shown.

4.4 Multi-fidelity Monte Carlo (MFMC) estimation

Finally, a multi-fidelity Monte Carlo estimation [7] (MFMC) implementation is examined within this illustrative example to showcase the benefits it can provide in seismic risk assessment applications. This approach leverages low computational cost, biased evaluations from a low-fidelity ROM to significantly accelerate the estimation process, and occasionally uses resources from the computationally expensive high-fidelity FEM, to establish an unbiased Monte Carlo (MC) estimation. This estimation will be used to replicate Fig.4, for structure S_2, for which large discrepancies were observed, especially for accelerations.

To better frame MFMC, let's first revisit the single-fidelity Monte Carlo (MC) estimation utilized in section 4.3 to compute $P[EDP>\beta]$. For either the FEM or ROM, and for each seismicity scenario, the estimate for the CCDF is given by

$$P_{FEM}^{MC}[EDP>\beta]=\frac{1}{N_q}\sum_{k=1}^{N_q} I[EDP_{FEM}^{k}>\beta] \quad \text{or} \quad P_{ROM}^{MC}[EDP>\beta]=\frac{1}{N_q}\sum_{k=1}^{N_q} I[EDP_{ROM}^{k}>\beta] \tag{12}$$

where N_q is the number of samples used in the estimation, EDP^k is the EDP sample for the k*th* seismic excitation, with subscript *FEM* and *ROM* used to distinguish between the two models, and $I[.]$ is the indicator function taking value equal to 1 if the relationship inside the brackets holds, else it is zero. The multi-fidelity Monte Carlo (MFMC) estimator for the CCDF, combines calculations by both models into a single MC estimation. It leverages the lower-fidelity ROM model to create a control variate to accelerate the MC estimation for the higher fidelity FEM. The MFMC estimation is ultimately expressed as [7]:

$$P_{FEM}^{MFMC}[EDP>\beta]=\frac{1}{N_{FEM}}\sum_{k=1}^{N_q} I[EDP_{FEM}^{k}>\beta] + a\cdot\left(\frac{1}{N_{ROM}}\sum_{k=1}^{N_q} I[EDP_{ROM}^{k}>\beta]-\frac{1}{N_{FEM}}\sum_{k=1}^{N_q} I[EDP_{ROM}^{k}>\beta]\right) \tag{13}$$

where a is the control variate parameter and N_{FEM} and N_{ROM} are the number of evaluations from the FEM and ROM respectively. This MFMC implementation provides always unbiased predictions with respect to the FEM risk estimates, correcting any potential challenges for the ROM accuracy, like the ones identified in the previous section for structure S_2. It also facilitates a reduction of the computational burden, expressed through a reduction of the variability (coefficient of variation) of the MC estimator, compared to an MC implementation that uses only the FEM. The number of simulations from each of the models and the value of the control variate are selected with objective to minimize exactly this variability of the MFMC estimator for a given computational budget. Denoting by $r=N_{ROM}/N_{FEM}$ the ratio of the number of model simulations, it can be shown [7], that the optimal value for this ratio is given by

$$r^{*}=\sqrt{\frac{c^{FEM}\cdot(\rho)^2}{c^{ROM}\left[1-(\rho)^2\right]}} \tag{14}$$

where ρ is the correlation coefficient of $I[EDP>\beta]$ between the FEM and ROM and c^{FEM} and c^{ROM} are the computational times needed for one analysis, for the FEM and ROM respectively. The optimal control variate a^{*} [7] is given by

$$a^{*}=\rho\sqrt{\frac{Var[I[EDP_{FEM}>\beta]]}{Var[I[EDP_{ROM}>\beta]]}} \tag{15}$$

where $Var[.]$ denotes variance. Finally, the efficiency of the MFMC estimation can be measured by the reduction of effort to achieve the same MC accuracy (i.e. estimator variability) compared to the MC estimation relying solely on the high-fidelity model. The reciprocal of these savings is termed as speed-up and denotes *sp* herein. It can be shown that it is given by

$$sp=\frac{c^{FEM}}{c^{FEM}+r\cdot c^{ROM}}\cdot\left[1-\left(1-\frac{1}{r}\right)\cdot\rho^2\right]^{-1} \tag{16}$$

It is evident from these equations that the overall efficiency of the MFMC implementation depends on both the computational efficiency of the ROM and its degree of correlation to the FEM, features that are explicitly optimized within the proposed ROM calibration scheme discussed in this paper.

In order to use the MFMC estimator to calculate the CCDF curves, the optimal r^{*} needs to be evaluated, for every EDP and every threshold. Since seismic risk assessment requires simultaneous estimation of the risk for multiple quantities of interest, it is highly impractical to calculate a different number of model evaluations for every estimation. Thus, in this example, the optimal r^{*} will be calculated only once, for a specific EDP, threshold β and seismicity scenario, and then use the same number of evaluations for all the other calculations. The optimal control variate a^{*} can be calculated for every

estimation case separately. Due to the fact that large discrepancies were observed for top-floor accelerations, for the lowest seismicity scenario examined (M=6.5, R=50km) and especially for $P[EDP > \beta] < 40\%$, acceleration is selected as the EDP for the MFMC estimation and the optimal r^* will be calculated for $P[EDP > \beta] = 20\%$, for the M=6.5, R=50 km scenario. Thus, the optimal ratio is found to be equal to 6.39. The number of ROM evaluations that are going to be used in the MFMC estimation is still 1000 and the FEM evaluation that are going to be included are $N_{FEM} = r^* \cdot N_{ROM} = 155$. Fig. 5 presents results for structures S_2 for first floor drift and top floor acceleration, in direct comparison to Fig. 4. Results in the figures show that the proposed MFMC approach facilitates excellent agreement with the high-fidelity FEM estimation, as expected. This is especially evident when compared to the results of Fig. 4, with the MFMC estimator providing for all thresholds and seismicity scenarios, excellent accuracy, close to the FEM estimation, even for the accelerations that were proven a great challenge earlier (results for drift even more consistent). In terms of the speed-up, for $P[EDP > \beta] = 20\%$, there is a 1.5 decrease in the computational time needed to gain the same level of accuracy for the top floor acceleration compared the a single MC estimation using evaluations from FEM. For other thresholds, and seismicity scenarios, approximately the same amount of speed-up is gained, even though r^* does not correspond to the optimal value. Especially for the inter-story drift ratios, more than 2.5-times the speed-up is gained. The reason this happens is evident from inspecting Eq. (16). If there is a strong correlation between the FEM and ROM (which is the case for drifts), the latter can provide accurate information about the former and when this is coupled with a substantial reduction in computational time that the low-fidelity model can provide, MFMC leverages the low-fidelity model many times and computational efficiency is gained. If the two models are weakly correlated, MFMC will utilize the low-fidelity model fewer times. For all the aforementioned reasons, implementation of the MFMC estimation for risk predictions for structure S_1 would have given greater speed-ups, due to the high correlation between FEM and ROM for all thresholds and seismicity scenarios.

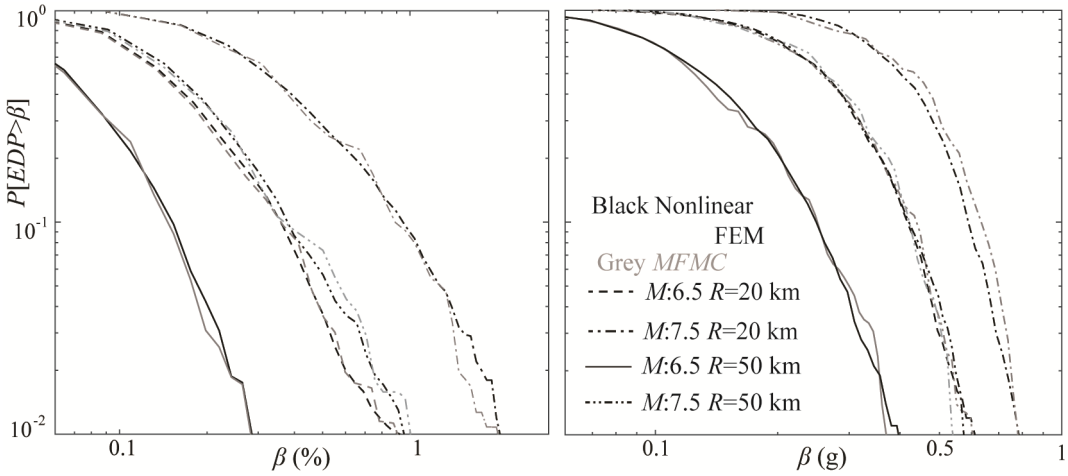

Fig.5: Comparison of CCDF curves from the high-fidelity OpenSees and the MFMC estimator corresponding to calibration D_1 for the ROM, for structure S_2. Results for selective seismicity scenarios and EDP_s are shown.

5. Conclusions

The calibration of reduced order hysteretic structural models and subsequent validation in seismic loss estimation setting was examined in this paper. The reduced order model (ROM) was developed using data from the original high-fidelity FEM. Static condensation was first used to obtain the stiffness matrix for the dynamic degrees of freedom (DoFs) and subsequently the restoring forces corresponding to the linear stiffness matrix were replaced by hysteretic ones, considering hysteretic spring connecting all DoF combinations. Different models were discussed for describing the hysteretic forces. Calibration was established by comparing nonlinear time-histories to the initial structural FEM, and a sequential optimization

was established to accommodate the adoption of complex descriptions for the reduced order model hysteretic forces. Validation within the illustrative example demonstrated the ability of the proposed reduced order modeling framework to offer, at a substantially reduced computational cost, a good match to the nonlinear FEM predictions for both the response to individual excitations, but more importantly, to risk predictions such as the vulnerability across different EDP thresholds for inter-story drifts and accelerations. Finally, a multi-fidelity MC implementation was examined. It was shown that this approach can be coupled well with the proposed reduced order modeling scheme to establishing efficient and unbiased risk estimation using data from both the FEM and the ROM.

6. References

[1] Haselton, C.B., et al., *An assessment to benchmark the seismic performance of a code-conforming reinforced-concrete moment-frame building.* Pacific Earthquake Engineering Research Center, 2008(2007/1).

[2] Gidaris, I. and A.A. Taflanidis, *Parsimonious modeling of hysteretic structural response in earthquake engineering: Calibration/validation and implementation in probabilistic risk assessment.* Engineering Structures, 2013. **49**: p. 1017-1033.

[3] Tehrani, M., et al., *Inelastic condensed dynamic models for estimating seismic demands for buildings.* Engineering structures, 2018. **177**: p. 616-629.

[4] Patsialis, D. and A. Taflanidis, *Reduced order modeling of hysteretic structural response and applications to seismic risk assessment.* Engineering Structures, DOI 10.1016/j.engstruct.2019.110135.

[5] Peherstorfer, B., P.S. Beran, and K.E. Willcox. *Multifidelity Monte Carlo estimation for large-scale uncertainty propagation*. in *2018 AIAA Non-Deterministic Approaches Conference*. 2018.

[6] Geraci, G., M.S. Eldred, and G. Iaccarino. *A multifidelity multilevel Monte Carlo method for uncertainty propagation in aerospace applications*. in *19th AIAA Non-Deterministic Approaches Conference*. 2017.

[7] Peherstorfer, B., K. Willcox, and M. Gunzburger, *Optimal model management for multifidelity Monte Carlo estimation.* SIAM Journal on Scientific Computing, 2016. **38**(5): p. A3163-A3194.

[8] Glasserman, P., *Monte Carlo Methods in Financial Engineering.* Springer, New York, 2004.

[9] Jones, D., M. Schonlau, and W. Welch, *Efficient global optimization of expensive black-box functions.* Journal of Global optimization, 1998. **13**: p. 455-492.

[10] Gill, P.E., et al., *User's guide for NPSOL (version 4.0): A Fortran package for nonlinear programming*. 1986, Stanford Univ CA Systems Optimization Lab.

[11] Golberg, D.E., *Genetic algorithms in search, optimization, and machine learning.* Addion wesley, 1989. **1989**(102): p. 36.

[12] McKenna, F., *OpenSees: A framework for earthquake engineering simulation.* Computing in Science and Engineering, 2011. **13**(4): p. 58-66.

[13] Kostic, S.M. and F.C. Filippou, *Section discretization of fiber beam-column elements for cyclic inelastic response.* Journal of Structural Engineering, 2011. **138**(5): p. 592-601.

[14] Ohtori, Y., et al., *Benchmark control problems for seismically excited nonlinear buildings.* Journal of Engineering Mechanics, 2004. **130**(4): p. 366-385.

[15] Filippou, F.C., V.V. Bertero, and E.P. Popov, *Effects of bond deterioration on hysteretic behavior of reinforced concrete joints.* 1983.

[16] Yassin, M.H.M., *Nonlinear Analysis of Prestressed Concrete Structures under Monotonic and Cycling Loads*. 1994, University of California, Berkeley.

[17] Filippou, F.C., E.P. Popov, and V.V. Bertero, *Effects of Bond Deterioration on Hysteretic Behavior of Reinforced Concrete Joints*. 1983, Earthquake Engineering Research Center,University of California, Berkeley.

[18] Chiou, B., et al., *NGA project strong-motion database.* Earthquake Spectra, 2008. **24**(1): p. 23-44.

[19] Vlachos, C., K.G. Papakonstantinou, and G. Deodatis, *Predictive model for site specific simulation of ground motions based on earthquake scenarios.* Earthquake Engineering & Structural Dynamics, 2018. **47**(1): p. 195-218.

